High performance, easy to fabricate, composite microheater for life sciences and biomedical applications.

Yudan Whulanza[1,2,], Husein Ammar[1], Deni Haryadi[1,3], Azizah Intan Pangesty[2,4], Widoretno Widoretno[5], Didik Tulus Subekti[5], and Jérôme Charmet [6*]*

1. Department of Mechanical Engineering, Faculty of Engineering, Universitas Indonesia, Depok 16424, Indonesia
2. Research Center for Biomedical Engineering, Universitas Indonesia, Indonesia
3. Department of Mechanical Engineering, Gunadarma University, Depok, Indonesia
4. Department of Metallurgical and Materials Engineering, Faculty of Engineering, Universitas Indonesia, Depok 16424, Indonesia
5. Research Organization for Health, National Research and Innovation Agency, Central Jakarta 10340, Indonesia
6. School of Engineering HE-Arc Ingénierie, HES-SO University of Applied Sciences Western Switzerland, 2000 Neuchâtel, Switzerland

E-mail (corresponding authors): yudan.whulanza@ui.ac.id, jerome.charmet@he-arc.ch

Keywords: composite materials, microheater, processing, heat cycle, DNA amplification.

Micro-heaters, are used in a number of applications including medical diagnostics[1–3], synthesis [4–6], environmental monitoring[7–9] and actuation[10–12]. Conventional micro-heaters rely on thin films electrodes microfabricated in clean-room environment [5,6,11]. However, low-cost alternatives based on conductive paste electrodes fabricated using printing techniques have started to emerge over the years[2,13–18]. Compared to thin film electrodes, such "thick" electrodes typically suffer from lower heating efficacy and poorer mechanical properties. Here we present a solution that addresses both issues simultaneously. Mixing silver ink and PVA results in the solubilization of performance-hindering organic compound that gets eliminated after heating. The new electrodes, which reach a temperature of 80 ºC within 5 minutes using a voltage of 1.0 V, display an overall 42% and 35% improvement of the mechanical (hardness) and electrical (resistivity) properties compared to pristine silver ink electrodes. To validate our results, we use the composite microheater to amplify and detect parasite DNA from Trypanosoma brucei, associated with African sleeping sickness. Our LAMP test compares well with commercially available systems, confirming the excellent performance of our microheaters. Since their fabrication relies on well-established techniques, we anticipate they will find use in a range of applications.

1. Introduction

Whether to control temperature dependent processes[2,19], drive actuators[11], or as part of sensing mechanisms[3,8,20], microheaters have found applications in chemical, food processing, automotive and aeronautic as well as biomedical and pharmaceutic industries to cite a few (see e.g. [ref. [8,16–18,21–23]]).

In addition to the obvious miniaturization aspects, microheaters have distinct advantages over their macroscale counterparts. An important feature is their superior operation efficiency when combined with resistive (or Joule) heating. The heating power $P = RI^2$, where I is the current passing through a conductor of resistance $R = \rho \cdot L/A$, can be written as:

$$P = \frac{\rho \cdot L \cdot I^2}{A} \quad (1)$$

Equation 1 highlights the heating power's dependency on the materials property (resistivity ρ) and geometry of the heating element (length L and cross section A). Therefore, for a given material, microheaters, manufactured using conventional microfabrication techniques, which typically enable the fabrication of long (centimetre scale) conductors with small (microscale) cross-section, are ideally suited to maximise heating power.

Another advantage of operating at the microscale is the increased surface to volume ratio that favours thermal transfer. We borrow examples from microfluidics where this feature is used to quickly heat-up solutions for example in DNA amplification (e.g. polymerase chain reaction[13,24] or loop-mediated isothermal amplification[2,22]) or for cell culture in bioreactors[25,26] but also in electrophoretic separation where large electric fields can be applied without excessive heating due to improved thermal dissipation under flow[27,28]. The above observations highlight the excellent performances of Joule-based microheating, which enables fast, precise and accurate control of temperatures with low power consumption, as confirmed in other studies[1,17].

In terms of dimensions, microscale cross-sections can be achieved through a combination of thin films deposition and structuring technique. A notable example is lift-off (which relies on a combination of physical vapour deposition and photolithography) to create microheaters of

cross sections typically of a few μm^2 (see e.g., ref [23]). In comparison, the smallest wires (gauge 40) have a cross-section of a few thousands μm^2, which corresponds to a decrease in heating power of the same factor (thousands fold) for the same materials and length (if one ignores the contribution of size-dependent losses[17]). This emphasizes the importance of the fabrication methods for the manufacturing of microheating elements. Yet, thin film deposition methods and photolithography that allow for very small cross sections, are usually limited to specialized laboratories[29]. This is mostly due to large investment and running costs. To overcome this limitation, low-cost alternatives have started to emerge.

More accessible methods to create low-cost microheaters include screen printing[17], doctor blade techniques[30], 3D printing[18] or even inkjet printing[2]. However, compared to their thin films counterparts, the heating elements (electrodes) usually have a larger cross section, reaching dimensions that are more comparable to conventional wires. Therefore, they lose some of the microscale size related advantages highlighted above, and in particular the heating power. In addition, such microheaters typically suffer from limited mechanical properties[1].

Here we resolve these limitations simultaneously through the development of nano-composite ink made of PVA and silver-ink. Microelectrodes from this nanocomposite can be deposited using doctor-blade techniques without alteration to the process parameters, with PVA concentrations up to 30% w/w. Interestingly, we show that heating cycles lead to a stable improvement of the electrical and mechanical properties, regardless of the PVA concentration. Improvements of 35% and 42% are noted for resistivity and hardness respectively for a nano-ink with 30% PVA, compared to pristine silver ink samples. We attribute these improvements to the loss of volatile organic compounds during the heating cycles, which favours the affinity between PVA and the silver ink in the processed samples. Systematic studies of the composite materials in their unprocessed (section 2.1) and processed conditions (sections 2.2 and 2.3 for the mechanical and electrical characterization) including after heating cycles (section 2.4) support this hypothesis. Finally, to validate our results, we demonstrate that our composite microheater produces results comparable to those of commercially available systems for the detection of the Trypanosoma brucei DNA using a LAMP test (section 2.5). Figure 1 shows an overview of the various geometries and characterization techniques applied herein.

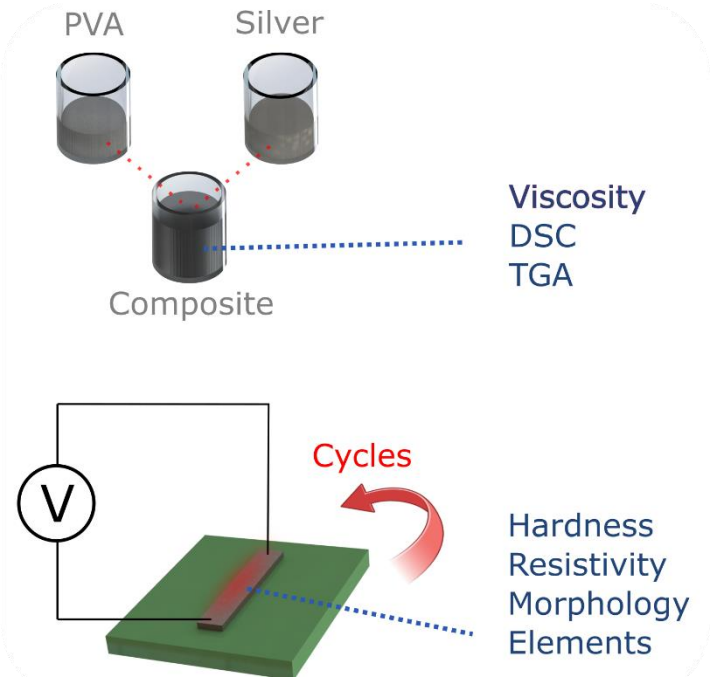

Figure 1. Overview of the project and materials characterisation. Tests were performed on the bulk, unprocessed material, on the processed (structured) material, before and after heating, including after a several cycles.

It is noted that other silver-based composites have been proposed in the context of electrical interconnects. One study shows that the partial replacement of silver particles by carbon black increases the scratch resistance of the resulting thick film and decreases the electrical resistivity[31]. Another paper describes the preparation of epoxy composites filled with nano- and micro-sized silver (Ag) particulate fillers and their effect on flexural properties, coefficient of thermal expansion, dynamic mechanical analysis, electrical conductivity, and morphological properties[32]. Other materials-focused publications highlight the enhanced properties of similar composites[33]. A notable example is that of a PDMS silver paste composited that was developed for better integration with PDMS based microfluidics chips[34]. However, none of the solutions reported above aimed at addressing the resistivity or mechanical issues let alone their combination, in the context of microheating.

The focus of this paper is on doctor blade techniques, but it is expected that the results can be adapted to other techniques including screen printing or inkjet printing. Overall, since our approach overcomes major limitations inherent to a range of low-cost microheater without adding any significant processing constraints, we anticipate that the results will be applicable to a broad range of situations.

2. Results and Discussion

2.1 Raw materials properties

To evaluate the effect of the PVA concentration on the bulk properties of the nano-composite ink, we first performed viscosity measurements. This was done using a Genero LVR rheometer with a gap dimension set to 0.328 mm and an upper plate of 7.935 mm radius. For the measurements, 1 mL of the nano-composite ink was used with shear rates between 20 s^{-1} and 200 s^{-1}.

Figure 2a shows that pristine silver ink has a higher viscosity coefficient than any of the composite nano-inks. The overall decrease in viscosity of the composites can be explained by the fact that PVA is widely used as a surfactant/dispersant in the synthesis of silver nanoparticles. The figure also shows that the viscosity value is not significantly affected by the PVA concentration (here, 10%, 20% and 30% w/w). We also note that the rheological curves show hysteresis, i.e., thixotropic behaviour, confirming results reported elsewhere[35].

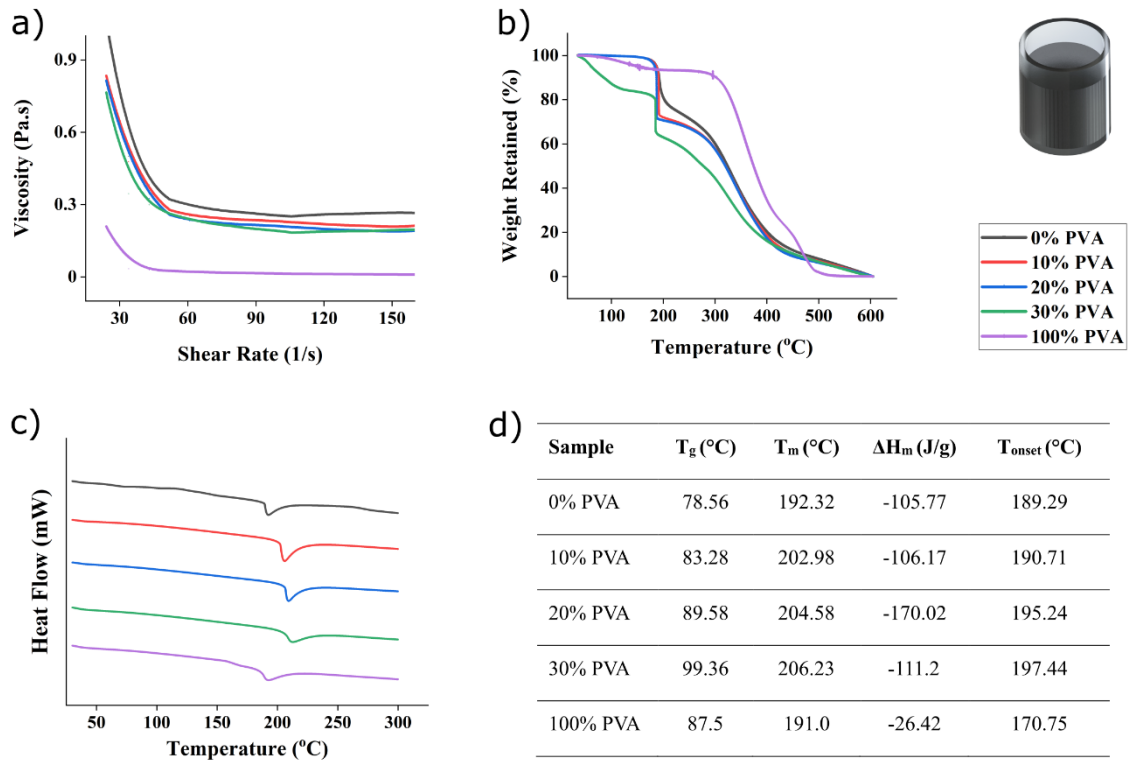

d)

Sample	T_g (°C)	T_m (°C)	ΔH_m (J/g)	T_{onset} (°C)
0% PVA	78.56	192.32	-105.77	189.29
10% PVA	83.28	202.98	-106.17	190.71
20% PVA	89.58	204.58	-170.02	195.24
30% PVA	99.36	206.23	-111.2	197.44
100% PVA	87.5	191.0	-26.42	170.75

Figure 2. Unprocessed samples characterization. a) Graph showing the viscosity of silver/PLA composite. Pristine silver ink (0% PVA) shows higher viscosity than samples with PVA (10%, 20% and 30%). b) Thermogravimetric analysis graph showing silver/PLA composite at various concentration. c) Result of differential scanning calorimetry (DSC) of the silver/PVA electrode with various PVA concentration. d) Data extracted from the DSC analysis (c) where T_g is the glass transition temperature; T_m the melting temperature; ΔH_m the materials melting enthalpy and T_{onset} the temperature of the onset of degradation.

Thermal Property Analyses

The thermal stability of the nanocomposite ink is evaluated using thermogravimetric analysis (TGA), which is used to determine the fraction of volatile components by measuring the weight change during heating. TGA thus provides information on the thermal behavior of materials, including thermal decomposition and pyrolysis. The measurements were carried out using a Perkin Elmer DTA 4000 instrument. Briefly, 15 mg of sample is placed in an aluminum pan and heated from room temperature to 600°C at a rate of 20°C/min under nitrogen atmosphere (30 ml/min). Figure 2b shows the TGA graphs of the nanocomposites against the pristine silver ink and PVA. The pristine PVA is fully degraded at 550°C, indicating a lower stability compared to the silver-based materials that degrade above 589°C. The nanocomposites follow the degradation curve of the pristine silver ink with 2 regions of interest. The evaporation of water is generally thought to be responsible for the changes observed in the first region, between 30 and 100°C. In the second region of interest, around 190°C, one observes different behaviors for each sample. Decomposition events are observed around 182 °C for the 30% PVA (39% weight loss), 186,5°C for sample 20% PVA (33% weight loss), 191.6°C for sample 10% PVA (29% weight loss), and 193.1°C for pure Ag, or 0% PVA (18% weight loss). In the same region, no distinct drop is noted for the pristine PVA, but overall, its weight loss is less than 10%.

The observations above show that thermal degradation increases with PVA concentration, with the 30% PVA composite showing the largest weight loss. However, the higher degradation rate of the composite between 150-200°C cannot be attributed to the excess PVA material alone as the pristine PVA (100%) has a lower weight loss than any other composites. Rather our results indicate that increasing PVA concentrations decreases the stability of the unprocessed composites, which confirm the trend observed with the viscosity measurements (Fig. 2a).

To complement the TGA measurements, we have performed differential scanning calorimetry (DSC) experiments. The measurements were performed on a Perkin Elmer DTA 4000 equipment, under nitrogen atmosphere (30 mL/min). Figure 2c shows the curves for all samples. Figure 2d recapitulates the values automatically generated by the software. They include the glass transition temperature T_g, the melting temperature T_m, the melting enthalpy ΔH_m and the temperature of the onset of degradation T_{onset}. Interestingly, the melting temperature of the pure silver nanoparticles paste (0% PVA) and the pristine PVA (100% PVA) are very close with 192.2 and 192.0 °C respectively, but these values increase for the nanocomposite. It reaches a maximum temperature of 206.2 °C for the 30% PVA sample. This is consistent with other

findings that indicate an increased interaction between silver nanoparticles and the hydroxyl groups of the PVA[36].

When comparing both techniques, the TGA results show an increased weight loss with PVA concentration whereas DSC shows an increased stability with PVA concentration. This may seem contradictory at first. But the TGA results may be explained by the presence of soluble compounds in the silver ink. Indeed, such a compound could be dissolved when mixing the aqueous PVA solution with the silver ink. There are a number of volatile compounds, including rosin, used in printing inks or solder reflux[37]. This behaviour would also explain the lower viscosity noted for composites with higher PVA concentration (see Fig. 2a). This hypothesis will be tested and discussed further in section 2.3 below. For the DSC results, it is interesting to note that the pristine silver ink and PVA have similar melting temperatures, but that it increases in the nanocomposites with increasing PVA concentration. This is thought to be due to the increased interaction between silver nanoparticles and hydroxyl of the PVA as noted previously[36].

2.2 Materials Processing

Having evaluated the bulk properties of the ink, we now investigate the properties of the materials after doctor-blade processing. We study the influence of PVA concentration on the dimension and hardness of test samples.

In our printing process, the ink filling and removal are operated at the same time by a doctor blade. An acrylic substrate is mounted onto the squeegee and the ink is transferred onto the substrate as the squeegee moves across the acrylic sheet. A circular test pattern was designed to evaluate the transfer process. Figure 3a shows results for silver 30% PVA nanocomposite. The transferred patterns show a good consistency with the original design despite the geometrical limitations inherent to colloidal systems as reported elsewhere[38].

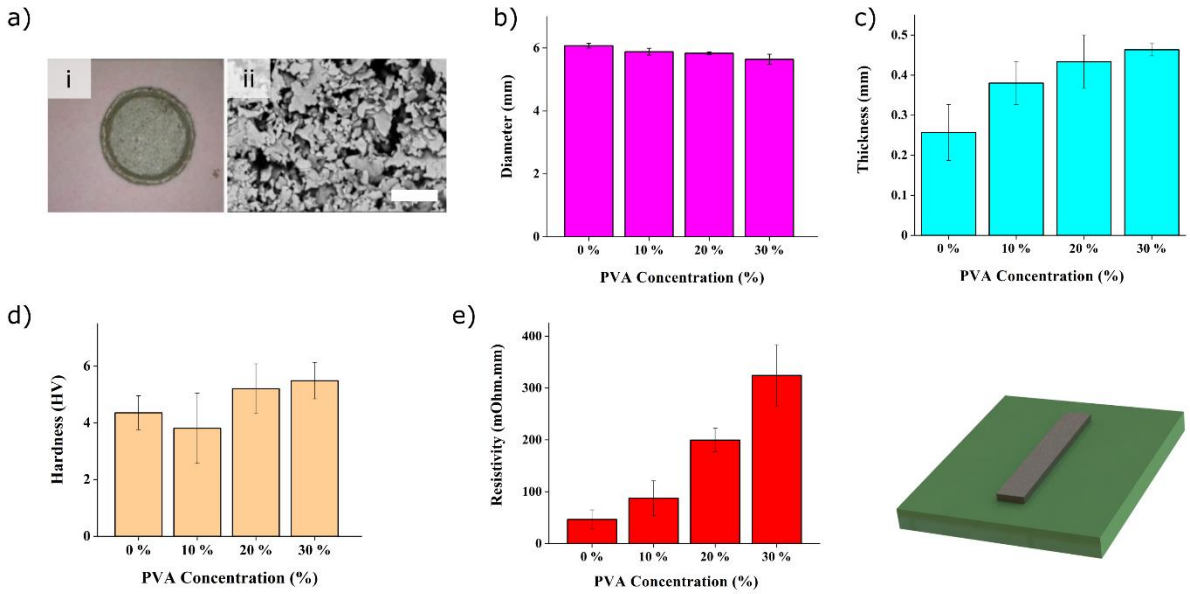

Figure 3. Processed samples characterisation. a) Optical image of the circular test pattern obtained with a silver 30% PVA nanocomposite (i) and Scanning electron micrograph showing detail of (i). The scale bar is 5 µm. b) Measurement of thickness and c) diameter of the printed silver electrode specimen with various concentrations of PVA. d) Vickers hardness of the electrode as a function of the PVA concentration. e) Resistivity of the nanocomposites of varying PVA concentrations from pristine silver ink (0% PVA) to 30% PVA nanocomposites.

The influence of the PVA concentration on the transferred geometry is depicted in figure 3b,c. An increase in PVA concentration results in a significantly thicker electrode and a slightly reduced diameter for the same doctor blade processing conditions. The average diameter of the 30% PVA pattern is approximately 6% lower compared to that of pristine silver pad (0% PVA), whereas its thickness shows almost a two-fold increase. Each set of dimensions for both conditions (30% vs 0% PVA) are significantly different as indicated by p-value of 0.007 and 0.008 for the diameter and thickness, respectively. The seemingly large standard deviations noted on the thickness values are in line with typical values reported using doctor blade techniques[39].

The increased interaction between the PVA and the Ag particles noted above and in ref.[36], could explain the geometrical results, whereby increased cohesive forces increases layer thickness during processing, and promotes lateral shrinkage upon drying.

Mechanical properties measurement

The effect of PVA on the specimen's mechanical properties were evaluated using Vickers microhardness measurements. Although a slight positive trend is observed, Figure 3d shows that the PVA concentration does not significantly alter the hardness compared to the pristine

silver sample (0% PVA) as indicated by one-way ANOVA (F=3.11, p=0.067) and confirmed by Tukey's test.

We postulate that the large hardness deviation observed is caused by the low homogeneity of the nanocomposite. Figure 3a clearly shows distinct areas of varying nanoparticles densities that will invariably produce different hardness values when hit by the micro-indenter.

2.3 Electrical characterisation and effect on materials properties

Electrical property measurement

The resistivity of the silver-PVA nanocomposite was measured using four-point probe technique as shown in Figure S1 in the supplementary materials. The results in Figure 3e shows, as expected, that the resistivity increases with the addition of non-conducting PVA. It increases exponentially, by approximately a factor 2 for each 10% PVA added, with a 7-fold increase to 0.33 mΩcm for the 30% PVA sample compared to the pristine silver ink.

The increase in resistivity is due to a combination of decrease in the percolation path due to a denser subphase that separates the conducting silver nanoparticles and the Coulomb blockade effect as demonstrated previously in similar composites[40].

Heating Characterization of Silver/PVA Electrode

To evaluate the performance of our nanocomposite as a heating element, we performed a series of measurement. First, we applied 1V across standard test microelectrodes with identical geometries (see details in the Methods section) but with varying PVA concentration and recorded their temperature every minute for 60 minutes. This measurement also enabled us to evaluate the nanocomposite electrode's time response and stability. The voltage value of 1 V was chosen based on previous research showing voltage breakdown at about 1.5 V on the same nanocomposite material[30]. Such phenomenon results in high currents that may damage the electrode.

As expected from the resistivity measurements (Fig 3e), the highest temperature after stabilization (about 110 °C) is achieved with the 30% PVA composite (see Fig. 4a). In the same conditions, it represents a 35% increase compared to the electrode made of pristine silver ink.

We also note that the stabilized temperature plateau increases with PVA concentration. In contrast, the temperature increase for the 10% PVA composite is only marginal compared to the pristine silver ink. When considering the resistivity measured above (Fig. 3e) together with the dimensional variations (Fig. 3b,c) and the fact that we are imposing a voltage (U) instead of a current ($P = U^2/R$), the temperature variations observed in Figure 4a match the calculated values within a 5% tolerance. Finally, it is interesting to note that it takes approximately 15 minutes to reach the plateau, independently of the PVA concentration. Then the temperature is stable for the remainder of the measurement (SD < 3%).

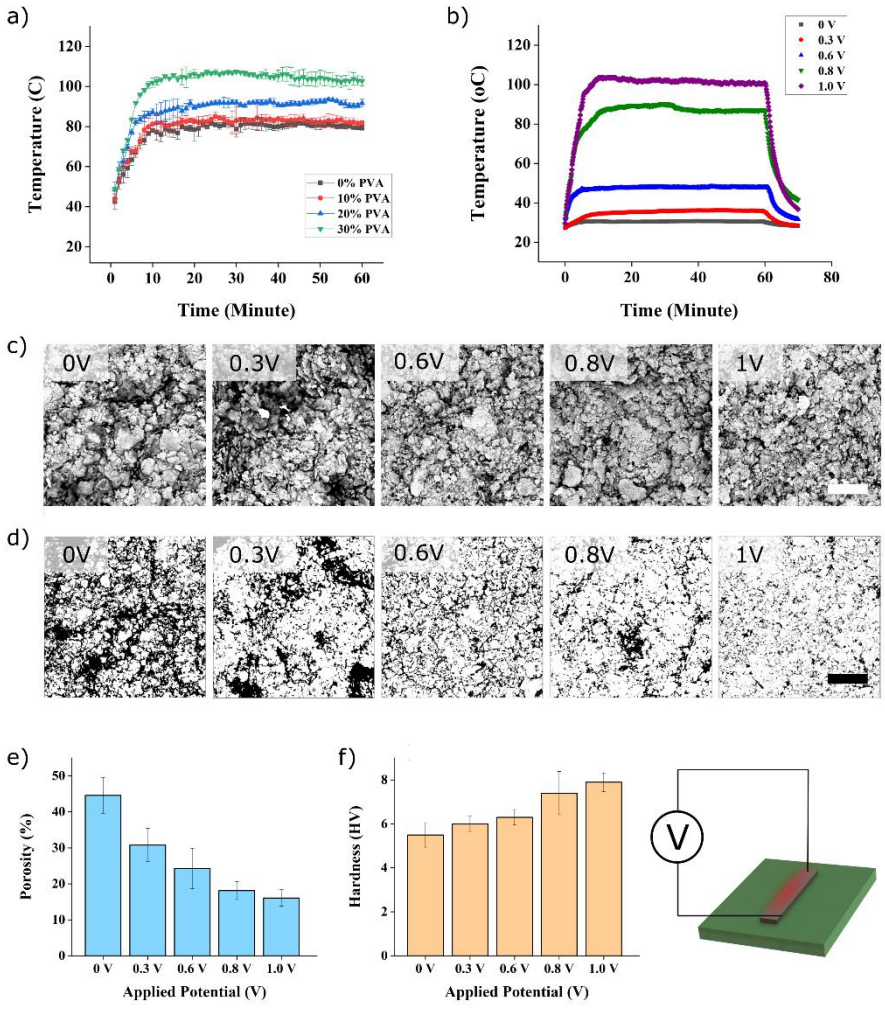

Figure 4. Processed samples characterisation. a) Measurement of temperature of nanocomposite microelectrodes with concentrations of PVA ranging from 0-30%. b) Application of varying voltage and effect on temperature on 30% PVA electrodes. Evaluation of the effect of voltage on the morphology of the 30% PVA electrodes using c) scanning electron micrograph of the nanocomposites after 60 minutes with a voltage applied between 0 and 1 V and d) visualization of porosity after image processing e) graph showing the quantified porosity based on the images, with 20 µm scale bars. (f) Hardness of the 30% PVA nanocomposite as a function of the applied voltage.

To investigate the influence of the voltage on the temperature, we performed a test on a standard 30% PVA microelectrode by applying voltages ranging from 0 to 1 V. The results can be seen in figure 8. Here again, the temperature increases proportionally with the voltage within a 5% tolerance, except for the value at 0.8 V, which should theoretically give 73 ± 4 °C. This difference is attributed to the fact that the sample was pre-heated (0.6V condition).

We used scanning electron microscopy to evaluate the morphology of the nanocomposites and the effect of the applied voltage (0 – 1 V) after 60 minutes. Figure 4c shows significant differences in silver microstructures for each of the different voltages. The micrographs seem to indicate that the nanocomposite becomes more compact with voltage. To verify this observation, we applied an image processing algorithm[40] to calculate the apparent porosity of the composites. Figure 4d shows the processed images. The apparent porosity (Fig. 4e) clearly decreases with the voltage, with a porosity value above 40% for the 0 V condition and less than 20% for the sample subjected to 0.8 V. The porosity content seems to plateau as it reaches 0.8 V. This is confirmed by ANOVA ($F = 28.00$, $p = 0.05$) and Tukey's test that show a significant difference between all samples except between the 0.8-1 V and 0.3-0.6 V.

To verify whether the observed change in porosity is due to the heat or to heat combined with electric current (Joule heating), we applied the porosity measurement algorithm after heating samples on a hot plate (i.e., without electric current). As for the samples heated by Joule heating, the porosity of hot plate heated sample decreases with the temperature. However, the absolute values are different, starting at about 60% for the room temperature condition and going down to 33% at 112 °C. In theory both room temperature conditions should give the same porosity (since no current or heat was applied to the samples) at this stage. The ~15% difference is attributed to the fact that each set of samples was prepared and measured on different days. Indeed, processing variability (for example drying time, due to variations in ambient temperature and humidity or SEM stability) could induce morphology changes or measurement artefacts. To account for these, we have truncated 15% from the hot-plate results (so that both starting porosity values are around 45%). By doing so, the porosity measurement for each heating condition matches within 12%, which suggests that the porosity change observed is due to heating only.

These results match the TGA results that correlates weight loss with temperature. We hypothesized above this weight loss was in part due to volatile compounds evaporating after

the heating cycles. The voids left by this "lost phase" could indeed lead to re-organization of the silver nanoparticles. This re-organization is further promoted by the strong interaction between the hydroxyl group of the PVA and the silver[36]. To confirm this hypothesis, we have performed energy-dispersive X-ray spectroscopy (EDX) to compare the normalized composition of a heating pad before and after application of 1V for 30 minutes (Table 1). Figure SM2 in supplementary materials shows the spectra. The results of the normalised weight concentration show that the relative silver level increases significantly with the application of voltage, while both carbon and oxygen levels decrease. Traces of gold were also noted and only change marginally after heating. This observation confirms the loss of organic volatile compounds (C, O) due to heating.

Table 1. Energy-dispersive X-Ray spectroscopy data show that the relative silver content (normalized weight concentration) increases while the carbon and oxygen concentration decrease after 1V has been applied to the electrode.

	0V	1V
Silver	52.84%	74.38%
Carbon	25.16%	11.54%
Oxygen	17.69%	8.58%
Gold	4.31%	5.50%

Finally, we measured the Vicker's hardness of the samples after the same treatments. Figure 4f shows that the hardness increases with the voltage. Using ANOVA ($F= 6.16$, $p= 0.004$) and Tukey's test we note that the samples at 0V and 1V show a significant difference, whereas there are not significant differences between the others. The hardness of the pristine sample (0V) is about 5.5 HV, while the sample biased to 1V reaches 7.8 HV, corresponding to a 42% improvement.

2.4 Performance after heat cycles.

Further experiments were performed to verify the heating performance of the nanocomposites after heating cycles (figure 5a,b). A tension of 1V was applied for 60 minutes to newly prepared samples. The measurement was repeated 5 times for each concentration, with enough time in between each measurement to allow the samples to return to room temperature, as confirmed using an infrared (IR) camera. Except for the pristine (0% PVA) silver ink, all other

nanocomposites produced similar temperature profile that show an increase in temperature for the first cycles, before stabilization after 3 cycles as shown in Figure 5a.

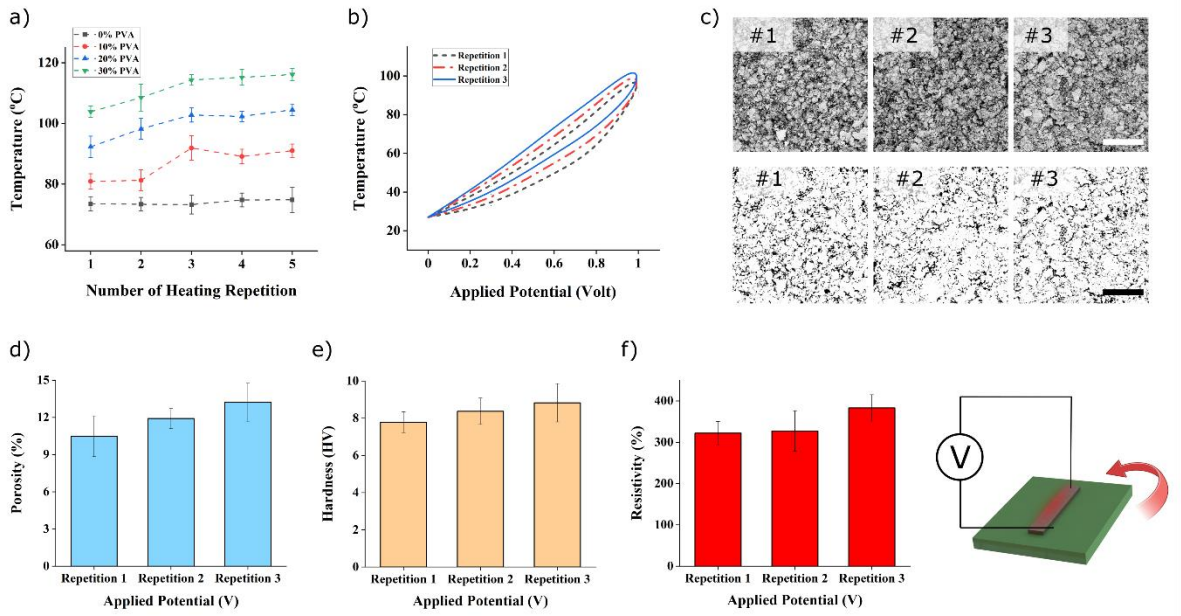

Figure 5. Sample characterisation after heating cycle of 30% PVA nanocomposite electrode. a) The temperature increases and then stabilises after heating cycles at 1 V up to 5 repetitions. b) The heating exhibits hysteresis as shown here for 3 cycles. c) Scanning electron microcographs showing the evolution of the samples' morphology after heating cycles. The scale bars are 20 µm Evolution of (d) the porosity, (e) the harness and (f) the resistivity of after heating cycles. as function of heating cycle.

Figure 5b shows the temperature as function of the voltage (ramp up from 0, 0.3, 0.6, 0.8 to 1V and then down to 0V again) applied for 60 minutes each. The hysteresis for each run indicates that the already heated sample has a better heating performance. This confirms the observation noted in Figures 4a,b and 4f. The overall heating performance increases after each cycle regardless of the voltage applied.

Figure 5c shows the SEM observation at the 1V step for the first three cycles. To extract meaningful information from the micrographs, we have used the porosity measurement algorithm introduced previously[40] (see Figure 5d). Using ANOVA (F= 3.97, p= 0.058) and Tukey's test there is no statistically significant difference between the cycles except between the first and the third one. Microhardness measurement was also performed to evaluate the effect of the cycles. Figure 5e shows the values obtained and ANOVA (F=1.77, p=0.226) with Tukey's test indicate that there is no significant difference in hardness between the different cycles. The same applies to the resistivity (Fig. 5f) that does not show any significant difference using ANOVA (F=2.42, p=0.170) and Tukey's test.

The results above indicate that the most significant performance improvement comes from the first heating cycle, and even though the overall trends are positive, the subsequent cycles only marginally improve the performance of the nanocomposite electrodes before stabilizing.

2.5 Validation using DNA amplification.

The final experiment, used to validate our composite microheater consisted in performing a LAMP test to amplify and detect DNA from Trypanosoma brucei, a parasite associated with African sleeping sickness. We applied a nanocomposite (30% PVA) heating electrodes on a commercially available chip, using doctor blade as described above and connected it to a DC power supply (See Fig. 6). The electrodes were subjected to three heating cycles to reach the optimal performance before the amplification step. After introducing the samples and reagents into the chip, we performed the isothermal amplification at 60 °C by applying 0.7 V, for 60 minutes. For comparison, we performed the same procedure on a commercial system. The detection of the amplified product was performed using gel electrophoresis (Fig. 6c). Our results show that our solution compares well with its commercial counterpart as a band around 100bp, corresponding to the expected 103bp amplicon, is visible in both cases. Negative and positive controls confirm the validity of our experimental approach.

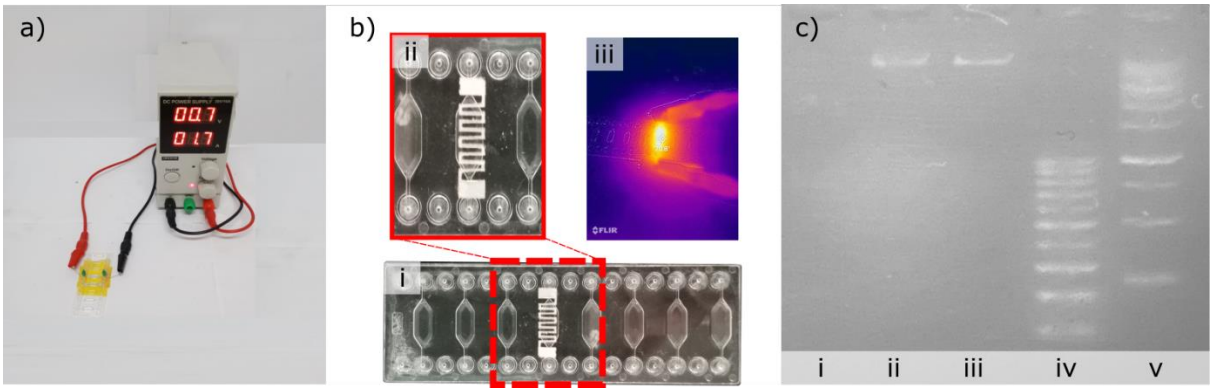

Figure 6. Validation of microheater for isothermal DNA amplification using LAMP procedure. a) shows the set-up used to heat the chip b) provides details of the electrodes on the chip (i,ii) as well as the measure of its heating using infrared camera (iii). c) shows the results from the LAMP process; where i and ii corresponds to the negative and positive controls on our chip, iii shows the positive control on a commercial system, and iv and v represent the ladders.

3. Conclusion

In this manuscript, we have demonstrated the development, characterization, and validation of a high-performance composite (PVA-silver ink) microheater deposited using doctor blade technique. We studied the composite in its unprocessed and processed form, including after heating cycles. We show that the electrical and mechanical performance of the microheater improve by 35% and 42% respectively after the first heating cycles. We attribute this

improvement to the loss of soluble organic compounds that dissolves from the silver ink in the aqueous PVA solution, and that evaporates upon heating as confirmed by EDX measurements. This leads to a stronger interaction between the silver and PVA[36] thereby increasing both the resistivity and the hardness of the electrodes. We validate the performance of the composite microheater by amplifying and detection DNA from Trypanosoma brucei, associated with African sleeping sickness. Our results compare well with existing and commercially available system and confirm the applicability of our microheater for healthcare applications. Overall, our results show that the silver ink – PVA composite can greatly enhance the performance of micro-heaters, and we anticipate that it will be used in a wide range of applications, since it relies on well-established -fabrication methods without additional constraints.

4. Experimental Section/Methods

Preparation of silver-pva ink. Firstly, a 0.01 g/mL solution of polyvinyl alcohol (PVA) was prepared by mixing a PVA pellet into distilled water. The mixture was then heated to 60^{o}C and stirred until complete dissolution of the pellet. Then, the solution was mixed with 1.5 grams of silver ink (MJ Chemical, Jakarta, Indonesia) to obtain mixtures of PVA/silver with concentrations of 10%, 20% and 30% w/w, referred to herein as 10% PVA, 20% PVA, and 30% PVA. Pristine silver ink is sometimes referred to as 0% PVA.

Preparation of PVA/silver heating pad. The silver ink was printed on acrylic substrate to create the heating electrodes using the doctor blade method[30]. Circular test patterns with a 6 mm diameter were designed for hardness measurement. Rectangular strip (5 x 30 mm) were used for the heating characterization (see Fig. SM3 in supplementary materials). These patterns were drawn using the Silhouette Studio v. 2.7.4 software and transferred to an adhesive vinyl film using an electronic craft cutter (Silhouette Cameo, Silhouette America, Inc.). The resolution was set to 300 DPI. Next, the patterned vinyl was attached to the acrylic chip. The doctor blade then applied the silver ink onto the substrate through the pattern while removing the excess ink. The ink was left to dry for 5 minutes before peeling off the vinyl. Finally, the ink was cured for 15 minutes at 120 °C on a hot plate.

Geometrical Measurement. A series of measurements were conducted to evaluate the dimension and morphology of the electrodes. The width of the electrodes was measured using a calibrated digital microscope Dinolite AM4113 (Anmo Taiwan). The thickness and contour of electrode was observed using an Accretech Surfcom 2900SD3 (Seimitsu Japan).

Micrographs of the silver electrodes surface were acquired using Scanning Electron Microscope Inspect F50 (FEI Japan) with magnifications of 200x and 1000x.

Electrical property measurement. The resistivity of our material was determined by measuring the resistance of electrodes of known dimensions using a four-point probe method (see Fig. SM1 for example of the set-up). The value of resistivity, defined as $\rho = RA/L$, plays an important role since it determines the temperature that can be dissipated due to the resistive (Joule) heating phenomenon.

Mechanical property measurement. Mechanical properties were evaluated using a universal tensile machine MCT series from A&D (Tokyo, Japan) with a maximum capacity of 500 N. The compression (mm) and load (N) were obtained at a crosshead speed of 1 mm/min and ended at 400 N of compression force.

Heating Performance Measurement. To generate heat through Joule heating effect, a DC power supply (GW Instek (Taipei, Taiwan)) was connected to the electrodes. The test was carried out at a constant potential. The resulting temperature change in the electrode was monitored using a four-channel data acquisition system. The temperature was monitored in real-time with NTC thermistor (TDK Electronics, Munich, Germany) connected to a data acquisition module from National Instrument NI-USB 6001 (Austin, USA). An infrared (IR) camera (FLIR Thermovision A320) (Santa Barbara, US) was used to confirm the measurement. See Fig. SM4 for a schematic of the set-up.

Porosity measurement. The porosity of microstructure was measured using an image processing method using automatic global (histogram-derived) thresholding reported previously[40]. The protocol consists of five step which are: (1) pixel size unit conversion to metric units; (2) image segmentation; (3) morphological filter to split connected pores; (4) verification step; (5) extraction of statistics from the detected pores. ImageJ is the primary software used for this study and analysis is performed on SEM images of 3D scaffolds. ImageJ is a public domain image-processing tool developed by the National Institutes of Health (ImageJ, 2018) was used to performed analyses on the SEM micrographs.

DNA Amplification using LAMP: A heating pad of 30% PVA-silver ink composite was deposited on a reaction chamber chip (Fluidic 584 series from Microfluidic Chipshop GmbH

(Jena, Germany). The chip was then connected to a DC power supply (GW Instek (Taipei, Taiwan) set to 0.7 V to reach 60°C for 60 minutes. The reactor chambers have a volume of 20 µL. The sample consist of a PCR Mix 10 µL (KODC-PCR reagent, Konimex, Solo, Indonesia), Primer Forward 1 µL (WOAH 2022), Primer reverse 1 µL (WOAH 2022). RNase free water 6 uL (KODC-PCR, Solo, Indonesia) and DNA sample 2 µL. Tripasonoma DNA was purchased from DNAzol Invitrogen, Waltham, USA. –Buffer was used as negative control. The temperature was set to 60°C for 60 minutes. A control amplification was performed on commercial thermocycler AllInOneCycler Bioneer (Daejeon, Korea) operated in the same conditions.

Gel electrophoresis: After PCR amplification, the amplification products were detected using agarose gel electrophoresis. 1KB DNA Ladder IV catalog number DL006 (Geneaid, Taiwan) and agarose powder catalog number PC0701 (Vivantis Technologies, Shah Alam, Malaysia) and Florosafe DNA stain catalog number BIO-5170 (1st Base, Singapore). For the staining of the agarose gel, loading dye catalog number HH 13701 (Geneaid Biotech, Taipei, Taiwan) was run at 80V for 30 minutes in the MUPID-exU electrophoresis system (Advance, Tokyo, Japan). The resulting gel images were captured by a camera. Transilluminator UVstar 8 (Analytik Jena, Jena, Germany) was used to read the gels. FLIR thermal camera was used to confirm the heating process.

Acknowledgements

The authors would like to acknowledge funding from: NKB-795/UN2.RST/HKP.05.00/2020 Nomor: 626/SK/R/UI/2020.

References

(1) Jeroish, Z. E.; Bhuvaneshwari, K. S.; Samsuri, F.; Narayanamurthy, V. *Microheater: Material, Design, Fabrication, Temperature Control, and Applications—a Role in COVID-19*; Springer US, 2022; Vol. 24. https://doi.org/10.1007/s10544-021-00595-8.

(2) Byers, K. M.; Lin, L. K.; Moehling, T. J.; Stanciu, L.; Linnes, J. C. Versatile Printed Microheaters to Enable Low-Power Thermal Control in Paper Diagnostics. *Analyst* **2020**, *145* (1), 184–196. https://doi.org/10.1039/c9an01546a.

(3) Chuang, H. S.; Wereley, S. Design, Fabrication and Characterization of a Conducting PDMS for Microheaters and Temperature Sensors. *Journal of Micromechanics and Microengineering* **2009**, *19* (4). https://doi.org/10.1088/0960-1317/19/4/045010.

(4) Cao, Y.; Wang, Z.; Liao, S.; Wang, J.; Wang, Y. A Light-Activated Microheater for the Remote Control of Enzymatic Catalysis. *Chemistry – A European Journal* **2016**, *22* (3), 1152–1158. https://doi.org/10.1002/CHEM.201503665.

(5) Lin, W. C.; Lin, Y. C.; Esashi, M.; Seshia, A. A. In-Situ Hydrothermal Synthesis of Zinc Oxide Nanostructures Using Microheaters. *IEEE Transactions on Nanotechnology* **2015**, *14* (6), 1046–1053. https://doi.org/10.1109/TNANO.2015.2468076.

(6) Kao, C.-C.; Su, Y.-K.; Hsieh, Y.-T.; -, al; Wang, C.-C.; Jenq, F.-L.; Liu, C.-C.; Huang, C.-Y.; Cheng, C.-Y.; Weng, C.-H.; Huang, C.-C.; Yeh, C.-S.; Lei, H.-Y.; Lee, G.-B. Synthesis of Hexagonal Gold Nanoparticles Using a Microfluidic Reaction System * Selective High Resistivity Region Formation by a Ni Catalyst on GaN Light-Emitting Diodes Color-Tunable Polymer Light-Emitting Diodes with Conjugated Polymer Homojunctions Synthesis of Hexagonal Gold Nanoparticles Using a Microfluidic Reaction System*. *Journal of Micromechanics and Microengineering JOURNAL OF MICROMECHANICS AND MICROENGINEERING J. Micromech. Microeng* **2008**, *18*, 8. https://doi.org/10.1088/0960-1317/18/3/035019.

(7) Rao, A.; Long, H.; Harley-Trochimczyk, A.; Pham, T.; Zettl, A.; Carraro, C.; Maboudian, R. In Situ Localized Growth of Ordered Metal Oxide Hollow Sphere Array on Microheater Platform for Sensitive, Ultra-Fast Gas Sensing. *ACS Applied Materials and Interfaces* **2017**, *9* (3), 2634–2641. https://doi.org/10.1021/ACSAMI.6B12677/ASSET/IMAGES/LARGE/AM-2016-12677B_0007.JPEG.

(8) Wu, J.; Wu, Z.; Ding, H.; Wei, Y.; Yang, X.; Li, Z.; Yang, B. R.; Liu, C.; Qiu, L.; Wang, X. Multifunctional and High-Sensitive Sensor Capable of Detecting Humidity, Temperature, and Flow Stimuli Using an Integrated Microheater. *ACS Applied Materials and Interfaces* **2019**, *11* (46), 43383–43392. https://doi.org/10.1021/ACSAMI.9B16336/ASSET/IMAGES/LARGE/AM9B16336_0006.JPEG.

(9) Long, H.; Harley-Trochimczyk, A.; He, T.; Pham, T.; Tang, Z.; Shi, T.; Zettl, A.; Mickelson, W.; Carraro, C.; Maboudian, R. In Situ Localized Growth of Porous Tin Oxide Films on Low Power Microheater Platform for Low Temperature CO Detection. *ACS Sensors* **2016**, *1* (4), 339–343. https://doi.org/10.1021/ACSSENSORS.5B00302/ASSET/IMAGES/LARGE/SE-2015-00302R_0004.JPEG.

(10) Darhuber, A. A.; Valentino, J. P.; Troian, S. M.; Wagner, S. Thermocapillary Actuation of Droplets on Chemically Patterned Surfaces by Programmable Microheater Arrays. *Journal of Microelectromechanical Systems* **2003**, *12* (6), 873–879. https://doi.org/10.1109/JMEMS.2003.820267.

(11) Qaiser, N.; Khan, S. M.; Babatain, W.; Nour, M.; Joharji, L.; Shaikh, S. F. F.; El-Atab, N.; Hussain, M. M. A Thermal Microfluidic Actuator Based on a Novel Microheater.

Journal of Micromechanics and Microengineering **2023**, *33* (3), 035001. https://doi.org/10.1088/1361-6439/ACB4A3.
(12) Vitale, W. A.; Petit, L.; Moldovan, C. F.; Fernández-Bolaños, M.; Paone, A.; Schüler, A.; Ionescu, A. M. Electrothermal Actuation of Vanadium Dioxide for Tunable Capacitors and Microwave Filters with Integrated Microheaters. *Sensors and Actuators A: Physical* **2016**, *241*, 245–253. https://doi.org/10.1016/J.SNA.2016.01.027.
(13) Wu, J.; Cao, W.; Wen, W.; Chang, D. C.; Sheng, P. Polydimethylsiloxane Microfluidic Chip with Integrated Microheater and Thermal Sensor. *Biomicrofluidics* **2009**, *3* (1), 012005. https://doi.org/10.1063/1.3058587.
(14) Carpini, G.; Lucarelli, F.; Marrazza, G.; Mascini, M. Oligonucleotide-Modified Screen-Printed Gold Electrodes for Enzyme-Amplified Sensing of Nucleic Acids. *Biosensors and Bioelectronics* **2004**, *20* (2), 167–175. https://doi.org/10.1016/J.BIOS.2004.02.021.
(15) Koh, C. G.; Tan, W.; Zhao, M. Q.; Ricco, A. J.; Fan, Z. H. Integrating Polymerase Chain Reaction, Valving, and Electrophoresis in a Plastic Device for Bacterial Detection. *Analytical Chemistry* **2003**, *75* (17), 4591–4598. https://doi.org/10.1021/AC0343836/SUPPL_FILE/AC0343836SI20030606_090544.PDF.
(16) Lin, J. L.; Wang, S. S.; Wu, M. H.; Oh-Yang, C. C. Development of an Integrated Microfluidic Perfusion Cell Culture System for Real-Time Microscopic Observation of Biological Cells. *Sensors 2011, Vol. 11, Pages 8395-8411* **2011**, *11* (9), 8395–8411. https://doi.org/10.3390/S110908395.
(17) Tiwari, S. K.; Bhat, S.; Mahato, K. K. Design and Fabrication of Screen Printed Microheater. *Microsystem Technologies* **2018**, *24* (8), 3273–3281. https://doi.org/10.1007/s00542-018-3821-6.
(18) Yin, M.; Xiao, L.; Liu, Q.; Kwon, S. Y.; Zhang, Y.; Sharma, P. R.; Jin, L.; Li, X.; Xu, B. 3D Printed Microheater Sensor-Integrated, Drug-Encapsulated Microneedle Patch System for Pain Management. *Advanced Healthcare Materials* **2019**, *8* (23), 1–10. https://doi.org/10.1002/adhm.201901170.
(19) Lin, W. C.; Yang, Y. J.; Hsieh, G. W.; Tsai, C. H.; Chen, C. C.; Liang, C. C. Selective Local Synthesis of Nanowires on a Microreactor Chip. *Sensors and Actuators A: Physical* **2006**, *130–131* (SPEC. ISS.), 625–632. https://doi.org/10.1016/J.SNA.2006.03.029.
(20) Ryu, S.; Yoo, I.; Song, S.; Yoon, B.; Kim, J. M. A Thermoresponsive Fluorogenic Conjugated Polymer for a Temperature Sensor in Microfluidic Devices. *Journal of the American Chemical Society* **2009**, *131* (11), 3800–3801. https://doi.org/10.1021/JA808077D/SUPPL_FILE/JA808077D_SI_001.PDF.
(21) Kan, W.; Chu, E.; Ren, W.; Liu, L.; Liu, W. Integrating NiCr-Based Thin Film Micro-Heater onto Electrode Header: A Review and Perspectives. *2021 IEEE International Conference on Advances in Electrical Engineering and Computer Applications, AEECA 2021* **2021**, 382–385. https://doi.org/10.1109/AEECA52519.2021.9574365.
(22) Uddin, S. M.; Sayad, A.; Chan, J.; Huynh, D. H.; Skafidas, E.; Kwan, P. Heater Integrated Lab-on-a-Chip Device for Rapid HLA Alleles Amplification towards Prevention of Drug Hypersensitivity. *Sensors 2021, Vol. 21, Page 3413* **2021**, *21* (10), 3413. https://doi.org/10.3390/S21103413.
(23) Singh, S.; Dinesh Kumar, •; Munish Vashishath, •; Singh, J.; Kumar Hooda, M. Investigation of CMOS Compatible Titanium Nitride-Based Microheater for Microthrusters. *ISSS Journal of Micro and Smart Systems 2022 11:2* **2022**, *11* (2), 417–426. https://doi.org/10.1007/S41683-022-00097-6.
(24) Moschou, D.; Vourdas, N.; Kokkoris, G.; Papadakis, G.; Parthenios, J.; Chatzandroulis, S.; Tserepi, A. All-Plastic, Low-Power, Disposable, Continuous-Flow PCR Chip with

Integrated Microheaters for Rapid DNA Amplification. *Sensors and Actuators B: Chemical* **2014**, *199*, 470–478. https://doi.org/10.1016/J.SNB.2014.04.007.
(25) Nieto, D.; McGlynn, P.; de la Fuente, M.; Lopez-Lopez, R.; O'connor, G. M. Laser Microfabrication of a Microheater Chip for Cell Culture Outside a Cell Incubator. *Colloids and Surfaces B: Biointerfaces* **2017**, *154*, 263–269. https://doi.org/10.1016/J.COLSURFB.2017.03.043.
(26) Lin, J. L.; Wu, M. H.; Kuo, C. Y.; Lee, K. Da; Shen, Y. L. Application of Indium Tin Oxide (ITO)-Based Microheater Chip with Uniform Thermal Distribution for Perfusion Cell Culture Outside a Cell Incubator. *Biomedical Microdevices* **2010**, *12* (3), 389–398. https://doi.org/10.1007/S10544-010-9395-4/FIGURES/7.
(27) Charmet, J.; Arosio, P.; Knowles, T. P. J. Microfluidics for Protein Biophysics. *Journal of Molecular Biology* **2018**, *430* (5), 565–580. https://doi.org/10.1016/J.JMB.2017.12.015.
(28) Urbano-Gámez, J. D.; Perdigones, F.; Quero, J. M. Semi-Automatic Lab-on-PCB System for Agarose Gel Preparation and Electrophoresis for Biomedical Applications. *Micromachines 2021, Vol. 12, Page 1071* **2021**, *12* (9), 1071. https://doi.org/10.3390/MI12091071.
(29) Charmet, J.; Rodrigues, R.; Yildirim, E.; Challa, P. K.; Roberts, B.; Dallmann, R.; Whulanza, Y. Low-Cost Microfabrication Tool Box. *Micromachines 2020, Vol. 11, Page 135* **2020**, *11* (2), 135. https://doi.org/10.3390/MI11020135.
(30) Whulanza, Y.; Ammarsyah, R.; Yatim, A. Characterization of Silver Resistive Electrode as Heating Module for Portable Thermocycler Device. *2021 IEEE International Biomedical Instrumentation and Technology Conference: The Improvement of Healthcare Technology to Achieve Universal Health Coverage, IBITeC 2021* **2021**, 40–45. https://doi.org/10.1109/IBITEC53045.2021.9649346.
(31) Leong, C. K.; Chung, D. D. L. Improving the Electrical and Mechanical Behavior of Electrically Conductive Paint by Partial Replacement of Silver by Carbon Black. *Journal of Electronic Materials* **2006**, *35* (1), 118–122. https://doi.org/10.1007/s11664-006-0193-y.
(32) Suriati, G.; Mariatti, M.; Azizan, A. Effects of Filler Shape and Size on the Properties of Silver Filled Epoxy Composite for Electronic Applications. *Journal of Materials Science: Materials in Electronics* **2011**, *22* (1), 56–63. https://doi.org/10.1007/S10854-010-0082-2/FIGURES/7.
(33) Mbhele, Z. H.; Salemane, M. G.; Van Sittert, C. G. C. E.; Nedeljković, J. M.; Djoković, V.; Luyt, A. S. Fabrication and Characterization of Silver-Polyvinyl Alcohol Nanocomposites. *Chemistry of Materials* **2003**, *15* (26), 5019–5024. https://doi.org/10.1021/CM034505A/ASSET/IMAGES/LARGE/CM034505AF00009.JPEG.
(34) Liu, L.; Peng, S.; Niu, X.; Wen, W. Microheaters Fabricated from a Conducting Composite. *Applied Physics Letters* **2006**, *89* (22), 2–5. https://doi.org/10.1063/1.2400065.
(35) Vincent, M.; Gopalakrishnan, V. K.; Sivanandan, S.; Radhika, T.; Raghu, N. Factors Influencing Rheological Characteristics of Silver Thick Film Paste and Its Correlation to Multilayer Ceramic Processing. *https://doi.org/10.1080/17436753.2018.1526435* **2018**, *118* (3), 106–113. https://doi.org/10.1080/17436753.2018.1526435.
(36) Sau, S.; Kundu, S. Variation in Structure and Properties of Poly(Vinyl Alcohol) (PVA) Film in the Presence of Silver Nanoparticles Grown under Heat Treatment. *Journal of Molecular Structure* **2022**, *1250*, 131699. https://doi.org/10.1016/J.MOLSTRUC.2021.131699.
(37) Sherman, K.; Mackay, C. A. A Thermoanalytical Study of the Components and Formulation of a Rosin Based Flux*.

(38) Walton, R. L.; Kupp, E. R.; Messing, G. L. Additive Manufacturing of Textured Ceramics: A Review. *Journal of Materials Research* **2021**, *36* (18), 3591–3606. https://doi.org/10.1557/s43578-021-00283-6.
(39) Gong, X.; Huang, K.; Wu, Y.-H.; Zhang, X.-S. Recent Progress on Screen-Printed Flexible Sensors for Human Health Monitoring. *Sensors and Actuators A: Physical* **2022**, *345*, 113821. https://doi.org/10.1016/j.sna.2022.113821.
(40) Hojat, N.; Gentile, P.; Ferreira, A. M.; Šiller, L. Automatic Pore Size Measurements from Scanning Electron Microscopy Images of Porous Scaffolds. *Journal of Porous Materials* **2023**, *30* (1), 93–101. https://doi.org/10.1007/S10934-022-01309-Y/FIGURES/10.

Supporting Information

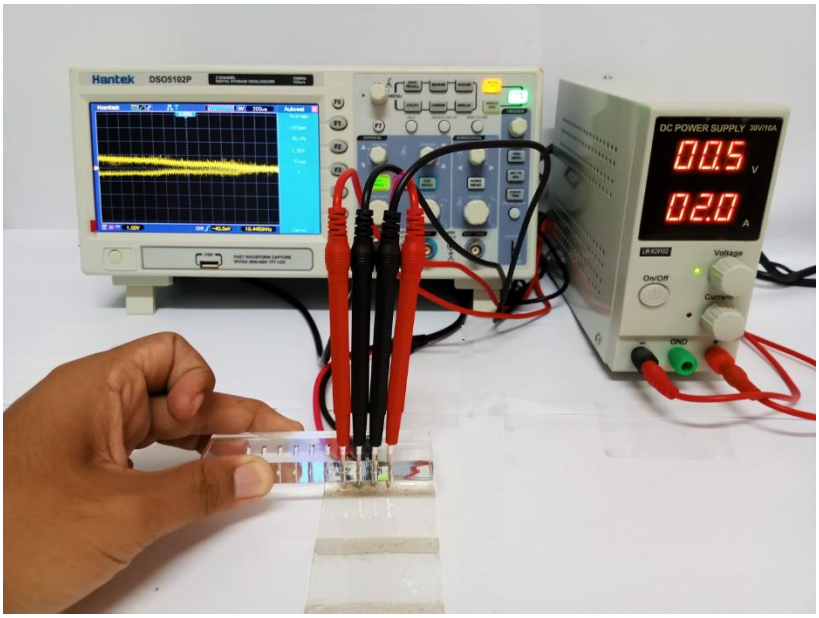

Figure SM1. Four-point probe measurement set-up to measure the resistivity of the electrodes

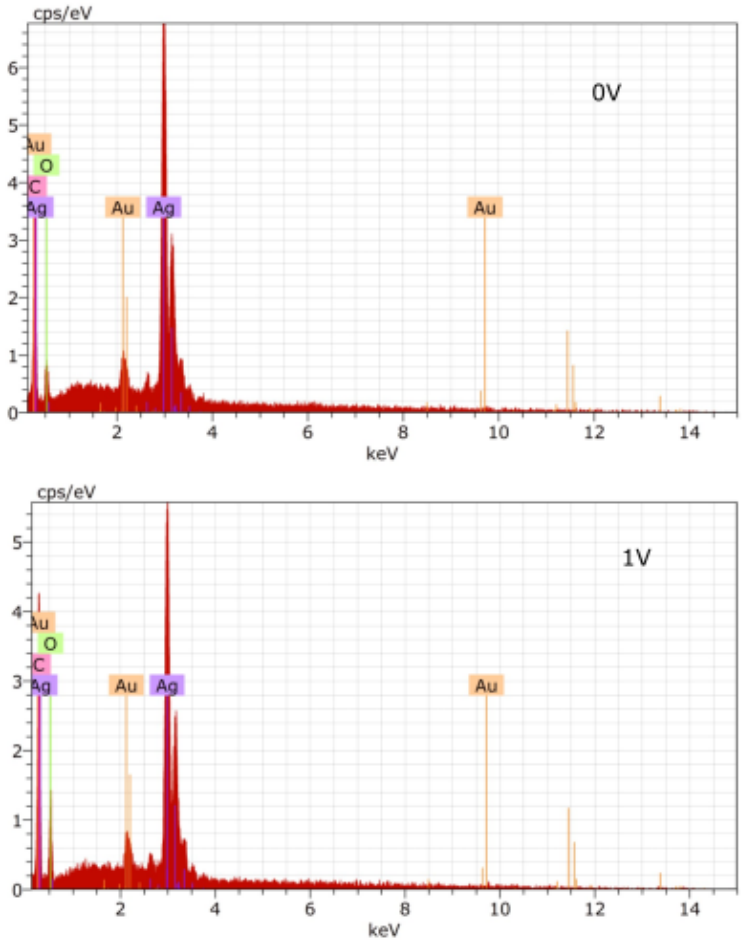

Figure SM2. Energy-dispersive X-Ray spectra of the pristine electrode (0 V, top) and after application of 1 V (bottom).

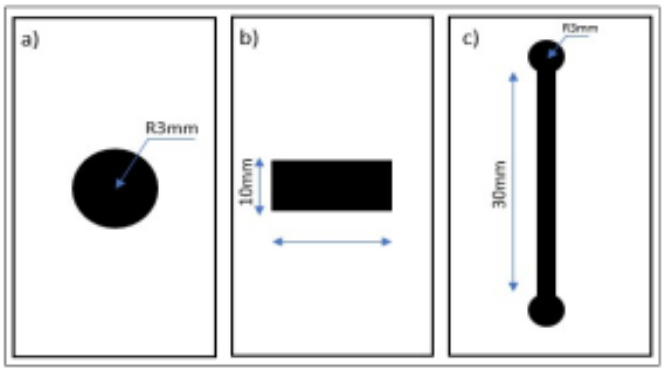

Figure SM3. Electrodes configuration used for the experiments.

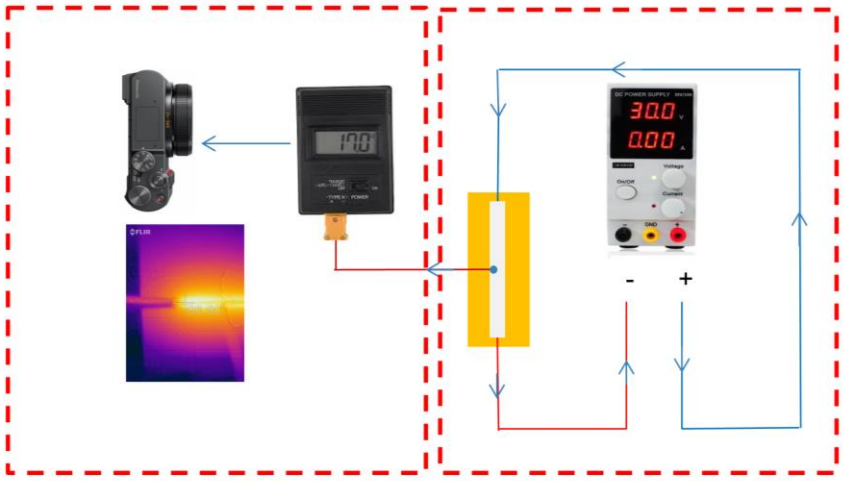

Figure SM4. Temperature measurement set-up during heating.